

Two-band density-matrix approach to nonlinear optics of excitons

I. Balslev

Fysisk Institut, Odense Universitet, DK-5230 Odense M, Denmark

R. Zimmermann

Zentralinstitut für Elektronenphysik, Akademie der Wissenschaften der Deutschen Demokratischen Republik, Hausvogteiplatz 5-7, DDR-1086 Berlin, German Democratic Republic

A. Stahl

Rheinisch-Westfälische Technische Hochschule, Aachen, D-5100 Aachen, Federal Republic of Germany
(Received 10 April 1989)

The two-band density-matrix dynamics of a semiconductor driven by an intense light field is set up in a real-space representation. The relation to the corresponding k -space theory is established. The real-space theory is applied to the case of excitonic resonances in a quantum well of finite width. Solutions describing the dynamical Stark effect are studied with particular emphasis on the following points: (i) the dependence of the measured signal on whether the spectral filtering of the probe beam is before or after the sample, and (ii) the influence of short pump pulses, the delay between the pump and the probe pulse, and the dephasing of the pump excitation. A perturbative analytical treatment and a real-time numerical integration of the relevant equations of motion are compared.

I. INTRODUCTION

Since the pioneering experiments of Fröhlich *et al.*,^{1,2} Mysyrowicz *et al.*,³ and Von Lehmen *et al.*⁴ much theoretical work has been devoted to the understanding of the nonlinear optical response of excitons in semiconductors, particularly the optical Stark effect. This effect is the modification of the excitonic absorption caused by an intense pump beam.

Most theoretical works in the field consider an adiabatic evolution of the system or even full stationarity. Such models are valid for long and spectrally narrow pulses. In this limit one must assume that the pump frequency is so far below the resonance that the dephasing of the pump excitation can be neglected. Beginning with Schmitt-Rink and Chemla⁵ a Hartree-Fock decoupling for electrons and holes in momentum representation has been widely used (dressed-atom approach).⁶⁻¹¹ The equivalence to a derivation starting with the exciton Hamiltonian¹² has been shown recently.¹³ More elaborate schemes using nonequilibrium Green's functions¹⁴⁻¹⁶ have also been reduced to (statically screened) Hartree-Fock terms.

Other works have emphasized the dynamics of the problem, i.e., have set up more or less approximate schemes which allow a study of the temporal evolution during the pump pulse. In the works by Balslev and Stahl¹⁷ the Coulomb interaction is treated approximately in that exchange integrals appearing in the equations of motion for the two-band density matrices are neglected. This approximation leads to a decomposition into isolated two-level systems. Correcting our earlier position,

we would like to stress that the full exchange must be taken into account. As was also overlooked in Refs. 11 and 12, the exchange terms are important even in the low-field limit. The work by Schäfer¹⁶ is free from this deficiency but uses an artificial pulse shape in the calculation. In general, the transformation of time-dependent field quantities such as the polarization into measurable quantities such as the optical transmission of a probe is not well understood in the literature. The importance of the specific experimental arrangement was emphasized in Ref. 13 in which two schemes used also in the present paper were introduced, namely spectral filtering of the probe pulse before or after the sample. Unlike the approach in Ref. 13 the present paper goes beyond the limit of low pump fields.

In the present work we shall report on a study which for the first time combines the accuracy of a full Hartree-Fock scheme with the advantage of a true dynamical approach. This is important when studying the influence of short pump pulses and finite dephasing of the pump excitation. The purposes of this paper are as follows.

(i) To compare the "dressed atom" approach of Schmitt-Rink, Haug, and co-workers with the two-band density-matrix approach in the form reported recently by Stahl¹⁸ including the Hartree terms in the equations of motion.

(ii) To utilize a real-space representation for treating the case of a quantum well with a width W comparable to the exciton Bohr radius.

(iii) To set up perturbative and nonperturbative calculating schemes for exploring the dependence of the optical Stark effect as a function of W and the detuning.

(iv) To study the influence of short pump pulses, dephasing of the pump excitation, the delay of the probe, and the position of a spectral filter (before or after the sample).

In Sec. II we present basic equations of motion for the interband and intraband density matrices including the exchange terms obtained in a Hartree-Fock treatment. Important simplifications are achieved in the limit of long electromagnetic waves and, at the same time, considering either a homogeneous system or an extended quantum well (Sec. III). In relation to a pump-and-probe experiment it is important to set up equations linearized with respect to the probe field and to specify the spectral filtering system used in the experiments (Sec. IV). In Sec. V it is demonstrated that the real-space density-matrix theory used in the present work becomes equivalent to related theories by Schmitt-Rink, Haug, and co-workers if the former approach is taken in the homogeneous, long-wavelength limit and proper attention is paid to the Fock terms. In Sec. VI are presented results from a perturbative and a nonperturbative, numerical treatment of the basic equations. These results include a number of novel features such as finite width of the quantum wells, finite spectral width and dephasing rate of the pump excitation, and noninstantaneous arrival of the two pulses.

II. TWO-BAND DENSITY-MATRIX THEORY: REAL-SPACE REPRESENTATION

Our model will be a direct-band-gap semiconductor idealized to have two parabolic, isotropic bands. The density matrix in a real-space representation is written as

$$\begin{aligned} \rho_{2B}(\mathbf{r}_1, \mathbf{r}_2, t) \\ = \begin{pmatrix} C(\mathbf{r}_1, \mathbf{r}_2, t) & Y^*(\mathbf{r}_1, \mathbf{r}_2, t) \\ Y(\mathbf{r}_1, \mathbf{r}_2, t) & \delta_B(\mathbf{r}_1 - \mathbf{r}_2) - D(\mathbf{r}_1, \mathbf{r}_2, t) \end{pmatrix}. \end{aligned} \quad (2.1)$$

C is the conduction-band submatrix, D is the valence band submatrix in the hole representation, Y is the interband density matrix, and δ_B is a suitably broadened delta function. Electromagnetic quantities derived from ρ_{2B} are the following:¹⁹ The monopolar charge density

$$\rho(\mathbf{r}) = -2e[C(\mathbf{r}, \mathbf{r}) - D(\mathbf{r}, \mathbf{r})], \quad (2.2)$$

the conduction current

$$\begin{aligned} j(\mathbf{r}) = 2 \frac{e\hbar}{2i} \iint \delta(\mathbf{r} - \mathbf{r}_1) \delta(\mathbf{r} - \mathbf{r}_2) (\nabla_1 - \nabla_2) \\ \times \left(\frac{C}{m_e} - \frac{D}{m_h} \right) d^3\mathbf{r}_1 d^3\mathbf{r}_2 \end{aligned} \quad (2.3)$$

and the interband polarization

$$P(\mathbf{r}) = M_0[Y(\mathbf{r}, \mathbf{r}) + Y^*(\mathbf{r}, \mathbf{r})], \quad (2.4)$$

m_e, m_h are effective masses, and M_0 is the dipole moment of the allowed transition. The prefactors 2 in (2.2) and (2.3) are due to the spin degeneracy which was not included in Ref. 19.

The electrodynamics of the system is described by equations of motion for ρ_{2B} in the presence of an electromagnetic field. The Hamiltonian generating the dynamics has the following form:

$$H = H_0 + H_{\text{Coulomb}} + \int (\rho\phi - jA - EP)d^3\mathbf{r}. \quad (2.5)$$

H_0 is the bare two-band Hamiltonian, H_{Coulomb} is the dielectrically screened Coulomb interaction specified by ϵ , and the electric field E is related to the potentials A, ϕ as usual:

$$E = -\partial_t A - \nabla\phi. \quad (2.6)$$

We shall here suppress the vectorial property of j, P, M_0, E , and A .

Applying the Hartree-Fock decoupling of the equations of motion one finds the following closed set of equations for the submatrices Y, C , and D :^{18,19}

$$\partial_t Y_{12} + i\Omega_{eh}Y_{12} + X_{12}^Y = \frac{iM_0}{\hbar}(E_1\delta_{12} - E_1C_{12} - E_2D_{21}), \quad (2.7)$$

$$\partial_t C_{12} + i\Omega_{ee}C_{12} + X_{12}^C = -\frac{iM_0}{\hbar}(E_1Y_{12} - E_2Y_{21}^*), \quad (2.8)$$

$$\partial_t D_{12} + i\Omega_{hh}D_{12} + X_{12}^D = -\frac{iM_0}{\hbar}(Y_{21}E_1 - Y_{12}^*E_2). \quad (2.9)$$

The numerical subscripts are abbreviations for coordinates in the sense $Y_{12} \equiv Y(\mathbf{r}_1, \mathbf{r}_2)$, etc. The Ω operators describing the propagation in the $(\mathbf{r}_1, \mathbf{r}_2)$ -configuration space under the influence of the potentials A, ϕ are¹⁸

$$\begin{aligned} \Omega_{eh} = \omega_g - \frac{V_{12}}{\hbar} + \frac{\hbar}{2m_h} \left(i\nabla_1 + \frac{e}{\hbar}A_1 \right)^2 \\ + \frac{\hbar}{2m_e} \left(i\nabla_2 - \frac{e}{\hbar}A_2 \right)^2 + \frac{e}{\hbar}(\phi_1^h - \phi_2^e), \end{aligned} \quad (2.10)$$

$$\begin{aligned} \Omega_{ee} = \frac{\hbar}{2m_e} \left[\left(i\nabla_2 - \frac{e}{\hbar}A_2 \right)^2 - \left(i\nabla_1 + \frac{e}{\hbar}A_1 \right)^2 \right] \\ + \frac{e}{\hbar}(\phi_1^e - \phi_2^e), \end{aligned} \quad (2.11)$$

$$\begin{aligned} \Omega_{hh} = \frac{\hbar}{2m_h} \left[\left(i\nabla_2 + \frac{e}{\hbar}A_2 \right)^2 - \left(i\nabla_1 - \frac{e}{\hbar}A_1 \right)^2 \right] \\ - \frac{e}{\hbar}(\phi_1^h - \phi_2^h). \end{aligned} \quad (2.12)$$

The direct Coulomb interaction

$$V_{12} = \frac{e^2}{4\pi\epsilon |\mathbf{r}_1 - \mathbf{r}_2|} \quad (2.13)$$

is included in Ω_{eh} while the remaining contributions from the Coulomb interaction are twofold, namely the exchange terms X^Y, X^C, X^D , and Hartree-type induced fields. The exchange terms are given by¹⁸

$$X_{12}^Y = \frac{i}{\hbar} \int (V_{13} - V_{23})(Y_{31}C_{32} - D_{31}Y_{32})d^3\mathbf{r}_3, \quad (2.14)$$

$$X_{12}^C = \frac{i}{\hbar} \int (V_{13} - V_{23})(Y_{31}^*Y_{32} + C_{13}C_{32})d^3\mathbf{r}_3, \quad (2.15)$$

$$X_{12}^D = \frac{i}{\hbar} \int (V_{13} - V_{23})(Y_{13}^*Y_{23} + D_{13}D_{32})d^3\mathbf{r}_3, \quad (2.16)$$

while the induced potential ϕ^{in} is given by

$$-e\phi^{\text{in}}(\mathbf{r}_1) = 2 \int V_{12}(C_{22} - D_{22})d^3\mathbf{r}_2. \quad (2.17)$$

When applying the Hartree-Fock decoupling [from Eq. (2.7) and on] the fields E , ϕ , and A are to be understood as self-consistent fields composed of external and induced fields.

The external part includes not only macroscopic external sources but also confining pseudopotentials from isoelectronic spatial structures. The latter contributions necessitate the distinction between ϕ^e and ϕ^h . Let us emphasize some properties of the dynamical equations (2.7)–(2.9).

(i) Equations (2.7)–(2.9) are a direct generalization of the optical two-level Bloch equations²⁰ to the case of a two-band system with electron-hole interaction. We shall denote these equations as the “band-edge equations” (BEE).

(ii) Within the approximation used there is a close relationship between the induced fields and the exchange terms: The induced fields represent the Hartree approximation responding to the total net charge and the exchange terms (2.17) are the corresponding Fock terms.²¹

(iii) The electric field E and the related potentials A, ϕ appear in a number of terms in the BEE. The most important one is the first term on the rhs of (2.7)–(2.9), driving Y linearly and thus responsible for the linear optical response.

(iv) As the diagonal parts X_{11}^C and X_{11}^D are zero, the diagonal parts $C(\mathbf{r}, \mathbf{r})$ and $D(\mathbf{r}, \mathbf{r})$ are driven by terms which in the long-wavelength limit become proportional to $E \text{Im}(y)$. These sources describe the build-up of electron-hole populations.

(v) The nonlinear dynamics of the band edge of a semiconductor is, according to the BEE, caused by three types of effects: (a) band-filling effects represented by the terms E_1C_{12} and E_2D_{21} on the right-hand side of (2.7), (b) effects from the exchange terms given in (2.14)–(2.16), and

(c) field-induced changes of the propagation via the appearance of A and ϕ in the Ω operators.

III. TRANSFORMATIONS RELEVANT FOR HOMOGENEOUS SYSTEMS OR QUANTUM WELLS IN THE LIMIT OF LONG ELECTROMAGNETIC WAVES

In their bilocal form the BEE are unique for studying nonhomogeneous systems such as the half-space problem¹⁹ and quantum wells.²² The bilocal structure is also essential for treating electromagnetic wavelengths which are not much longer than the quantum coherence lengths involved.

On the other hand, the treatment of the full dimensionality of the configuration space is very demanding, and so there are strong motivations for approximations leading to a reduced dimensionality.

Before introducing such simplifications we shall first transform the BEE in such a way that the vector potential \mathbf{A} is removed from the propagation operators. We substitute as follows:

$$Y_{12} = \tilde{Y}_{12}e^{ie(\mathbf{A}_1 \cdot \mathbf{r}_1 - \mathbf{A}_2 \cdot \mathbf{r}_2)/\hbar}, \quad (3.1)$$

$$C_{12} = \tilde{C}_{12}e^{ie(\mathbf{A}_1 \cdot \mathbf{r}_1 - \mathbf{A}_2 \cdot \mathbf{r}_2)/\hbar}, \quad (3.2)$$

$$D_{12} = \tilde{D}_{12}e^{-ie(\mathbf{A}_1 \cdot \mathbf{r}_1 - \mathbf{A}_2 \cdot \mathbf{r}_2)/\hbar}. \quad (3.3)$$

Using the Coulomb gauge it can be shown that the functions $\tilde{Y}, \tilde{C}, \tilde{D}$ obey the BEE with Ω operators replaced by the following operators with tildes:

$$\begin{aligned} \tilde{\Omega}_{eh} = & \omega_g - \frac{\hbar}{2m_h} \nabla_1^2 - \frac{\hbar}{2m_e} \nabla_2^2 \\ & + \frac{e}{\hbar} (\phi_1^h - \mathbf{r}_1 \cdot \mathbf{E}_1^t - \phi_2^e + \mathbf{r}_2 \cdot \mathbf{E}_2^t), \end{aligned} \quad (3.4)$$

$$\begin{aligned} \tilde{\Omega}_{ee} = & \frac{\hbar}{2m_e} (\nabla_1^2 - \nabla_2^2) + \frac{e}{\hbar} (\phi_1^e - \mathbf{r}_1 \cdot \mathbf{E}_1^t - \phi_2^e + \mathbf{r}_2 \cdot \mathbf{E}_2^t), \end{aligned} \quad (3.5)$$

$$\begin{aligned} \tilde{\Omega}_{hh} = & \frac{\hbar}{2m_h} (\nabla_1^2 - \nabla_2^2) - \frac{e}{\hbar} (\phi_1^h - \mathbf{r}_1 \cdot \mathbf{E}_1^t - \phi_2^h + \mathbf{r}_2 \cdot \mathbf{E}_2^t) \end{aligned} \quad (3.6)$$

where $\mathbf{E}^t = -\dot{\mathbf{A}}$ is the transverse component of the electric field.

Let us first consider a homogeneous system. In this case Y, C , and D depend only on the relative coordinate, and the potentials ϕ^e and ϕ^h are equal. Furthermore, in the long-wavelength limit E, A , and ϕ vary little over the spatial extent of Y, C , and D in relative space. This simplifies the band-edge equations considerably:

$$\begin{aligned} & \left(-i\hbar\partial_t + \hbar\omega_g - \frac{\hbar^2}{2\mu}\nabla^2 - e\mathbf{E}\cdot\mathbf{r} - V(\mathbf{r}) \right) \tilde{Y}(\mathbf{r}) + \int [V(\mathbf{r}') - V(\mathbf{r}' - \mathbf{r})][\tilde{Y}(\mathbf{r}')\tilde{C}(\mathbf{r} - \mathbf{r}') - \tilde{C}(\mathbf{r}')\tilde{Y}(\mathbf{r}' - \mathbf{r})]d^3\mathbf{r}' \\ & = M_0[\delta(\mathbf{r}) - 2\tilde{C}(\mathbf{r})]E - i\hbar\partial_t\tilde{C}(\mathbf{r}) + \int [V(\mathbf{r}') - V(\mathbf{r}' - \mathbf{r})]\tilde{Y}^*(-\mathbf{r}')\tilde{Y}(\mathbf{r} - \mathbf{r}')d^3\mathbf{r}' \end{aligned} \quad (3.7)$$

$$= -M_0[\tilde{Y}(\mathbf{r}) - \tilde{Y}^*(-\mathbf{r})]E. \quad (3.8)$$

Here μ is the reduced mass and the space coordinates \mathbf{r} and \mathbf{r}' refer to the relative space. We have used the fact that there is no net charge, which implies that $D(\mathbf{r}) = C(-\mathbf{r})$. We have neglected the influence of the electric field on Ω_{ee} because such a term gives rise to Drude-like nonresonant response. As a consequence of this, C becomes real, and so the CC term in the integral in (2.15) vanishes.

Studying optical processes we are interested in the interband polarization [Eq. (2.4)] involving Y_{11} . As $Y_{11} = \tilde{Y}_{11}$ there is no need for the distinction between quantities with and without tildes. Consequently, we shall drop the tildes in the rest of the present paper and still use equations of the type of (3.7) and (3.8).

In the transformed version (3.7) of the BEE it becomes manifest that the longitudinal electric field and the transverse electric field exert the same influence on the propagation of quantum-mechanical waves. The field-induced modification of the propagation [lhs of (3.7)] gives rise to the static Stark effect and the infrared resonant Stark effect studied by Fröhlich *et al.*,^{1,2,22} while the band-filling terms on the rhs of (3.7) give rise to the optical Stark effect appearing for near-band-gap frequencies. In this

work we shall concentrate on the latter effect and so we can neglect the electric field on the lhs of (3.7).

Next we consider a quantum well. If its width is smaller than a few exciton Bohr radii (growth direction parallel to the z axis) one may approximate Y , C , and D as follows:

$$Y_{12} = u_h(z_1)u_e(z_2)Y(\rho), \quad (3.9)$$

$$C_{12} = u_e(z_1)u_e(z_2)C(\rho), \quad (3.10)$$

$$D_{12} = u_h(z_1)u_h(z_2)D(\rho), \quad (3.11)$$

where ρ is the projection on the (x, y) plane of the relative space coordinate, and u_e, u_h are normalized confinement wave functions of the considered sublevel. The conditions for the approximation of (3.9)–(3.11) are (i) that the exciton binding energy is small compared with the spectral separation between different sublevel pairs and (ii) that the Fröhlich-type Stark effect can be neglected.²² Applying the long-wavelength approximation we obtain after integrating over the z coordinates:

$$\begin{aligned} & \left(-i\hbar\partial_t + \hbar\omega'_g - \frac{\hbar^2}{2\mu}\nabla_\rho^2 - v(\rho) \right) Y(\rho) + 2 \int [v(\rho')Y(\rho')C(\rho' - \rho) - \bar{v}(\rho')C(\rho')Y(\rho' - \rho)]d^2\rho' \\ & = m_0E[\delta(\rho) - 2C(\rho)] - i\hbar\partial_t C(\rho) + \int v(\rho')[Y^*(\rho')Y(\rho' - \rho) - Y(\rho')Y^*(\rho' - \rho)]d^2\rho' \end{aligned} \quad (3.12)$$

$$= -m_0E[Y(\rho) - Y^*(-\rho)], \quad (3.13)$$

where

$$m_0 = M_0 \int u_e(z)u_h(z)dz, \quad (3.14)$$

E_ρ is the field component in the (x, y) plane, and ω'_g is the gap frequency associated with the actual pair of quantum-well sublevels.

As shown in Appendix A the potential functions $v(\rho)$ and $\bar{v}(\rho)$ depend on the width W of the quantum well and the confinement sublevel in question. In the simple case of infinitely high confining barriers and common index n of the sublevels we have

$$v(\rho) = \bar{v}(\rho) = \frac{e^2}{4\pi\epsilon} \int_0^1 dt \frac{1}{(\rho^2 + W^2t^2)^{1/2}} \left[(1-t) \left(2 + \cos(2\pi nt) + \frac{3}{2\pi n} \sin(2\pi nt) \right) \right]. \quad (3.15)$$

This potential is Coulomb-like ($\propto 1/\rho$) for $\rho \gg W$ and logarithmic for $\rho \ll W$. It is important to note that in situations other than this, the Hartree-type induced fields must be included. One way of doing this is to include a Hartree term in the potential $\bar{v}(\rho)$ (see Appendix A).

IV. LINEARIZATION WITH RESPECT TO A PROBE FIELD

We shall consider the strong pump with a known time dependence of the field $E_{\text{pm}}(t)$ leading to the densities Y, C . The addition of a weak probe field $E_{\text{pr}}(t)$ gives rise to changes $\delta Y, \delta C$. We shall assume that E_{pr} is so small that the relations between $\delta Y, \delta C$, and E_{pr} are linear. The linearized equation becomes

$$\begin{aligned} & \left(-i\hbar\partial_t + \hbar\omega'_g - \frac{\hbar^2}{2\mu}\nabla_\rho^2 - v(\rho) \right) \delta Y(\rho) + 2 \int v(\rho') [\delta Y(\rho') C(\rho' - \rho) + Y(\rho') \delta C(\rho' - \rho)] d^2\rho' \\ & - 2 \int \bar{v}(\rho') [\delta C(\rho') Y(\rho' - \rho) + C(\rho') \delta Y(\rho' - \rho)] d^2\rho' \\ & = m_0 E_{\text{pr}} [\delta(\rho) - 2C(\rho)] - 2m_0 E_{\text{pm}} \delta C(\rho) \\ & - i\hbar\partial_t [\delta C(\rho)] + \int v(\rho) [\delta Y^*(\rho') Y(\rho' - \rho) - \delta Y(\rho') Y^*(\rho' - \rho)] d^2\rho' \\ & + \int v(\rho') [Y^*(\rho') \delta Y(\rho' - \rho) - Y(\rho') \delta Y^*(\rho' - \rho)] d^2\rho' \end{aligned} \quad (4.1)$$

$$= -m_0 E_{\text{pr}} [Y(\rho) - Y^*(-\rho)] - m_0 E_{\text{pm}} [\delta Y(\rho) - \delta Y^*(-\rho)], \quad (4.2)$$

where Y and C are solutions to (3.12) and (3.13) with $E = E_{\text{pm}}$.

In relation to experiments we shall assume that suitable spatial filtering allows the detection of $\delta P \propto \delta Y(0)$ without admixture of $P \propto Y(0)$ from the pump. We shall concentrate on the relative absorption $-\Delta I/I$ of the probe light. If the transmitted light is filtered through a monochromator the detected quantity is

$$\left(-\frac{\Delta I(\omega)}{I(\omega)} \right)_{\text{filtered}} \propto \frac{\text{Im}[E_{\text{pr}}^* \omega \delta Y^\omega(0)]}{|E_{\text{pr}}^\omega|^2}, \quad (4.3)$$

where the superscript ω refers to a Fourier transformation. Without a monochromator after the sample, the relevant quantity is

$$\left(-\frac{\Delta I}{I} \right)_{\text{unfiltered}} \propto \frac{\int dt \text{Im}[E_{\text{pr}}^* \delta Y(0)]}{\int dt |E_{\text{pr}}|^2}. \quad (4.4)$$

In realistic applications of the BEE one must include irreversible dephasing processes. Simplest is a T_2 -like relaxation obtained by replacing $\partial_t Y$ by $\partial_t Y + \Gamma Y$. As the actual absorption near the exciton lines has a line shape very different from a simple Lorentzian, one should use two different dephasing rates, one for the dephasing of the probe excitation Γ_{pr} to be inserted into (4.1) and one for the pump excitation Γ_{pm} to be inserted in (4.1).

V. CONNECTION TO RELATED THEORIES

So far we have worked in real space. Since most other papers in the field use a \mathbf{k} -space representation we Fourier transform the basic equations with respect to space in order to compare more directly with other works. We shall concentrate on the two-dimensional case. Then we use

$$n(\mathbf{k}) = \int d^2\rho C(\rho) e^{i\mathbf{k}\cdot\rho}, \quad P(\mathbf{k}) = \int d^2\rho Y(\rho) e^{i\mathbf{k}\cdot\rho}. \quad (5.1)$$

The change in notation ($C \rightarrow n$ for pair density, $Y \rightarrow P$ for the polarization) should further help to compare with the literature. The set of differential equations becomes

$$\left(-i\hbar\partial_t + \mathcal{E}_e(\mathbf{k}) + \mathcal{E}_h(\mathbf{k}) - 2 \sum_{\mathbf{k}'} \bar{v}(\mathbf{k} - \mathbf{k}') n(\mathbf{k}') \right) P(\mathbf{k}) - [1 - 2n(\mathbf{k})] \sum_{\mathbf{k}'} v(\mathbf{k} - \mathbf{k}') P(\mathbf{k}') = m_0 E [1 - 2n(\mathbf{k})], \quad (5.2)$$

$$-i\hbar\partial_t n(\mathbf{k}) + \sum_{\mathbf{k}'} v(\mathbf{k} - \mathbf{k}') [P^*(\mathbf{k}') P(\mathbf{k}) - P(\mathbf{k}') P^*(\mathbf{k})] = -m_0 E [P(\mathbf{k}) - P^*(\mathbf{k})] \quad (5.3)$$

where $\mathcal{E}_e(k), \mathcal{E}_h(k)$ are the free-particle energies [$\mathcal{E}_e(k) + \mathcal{E}_h(k) = \hbar\omega'_g + \hbar^2 k^2/2\mu$]. The term containing \bar{v} is the Hartree-Fock self-energy of electrons and holes, and the prefactor $(1 - 2n)$ describes the phase-space filling which acts to reduce the exciton binding as well as the coupling to light. Equations (5.2) and (5.3) are identical to the equations derived by Schmitt-Rink and co-workers^{5,6} based on the Hamiltonian H in \mathbf{k} -space (here applied to a quantum-well situation with an isolated pair of sublevels):

$$\begin{aligned}
H = & \sum_{\mathbf{k}} \mathcal{E}_e(\mathbf{k}) c_{\mathbf{k}}^{\dagger} c_{\mathbf{k}} + \mathcal{E}_h(\mathbf{k}) v_{\mathbf{k}}^{\dagger} v_{\mathbf{k}} - m_0 E (c_{\mathbf{k}}^{\dagger} v_{\mathbf{k}} + v_{\mathbf{k}}^{\dagger} c_{\mathbf{k}}) \\
& + \frac{1}{2} \sum_{1234} [V_{ee}(\mathbf{k}_1 - \mathbf{k}_4) c_1^{\dagger} c_2^{\dagger} c_3 c_4 + V_{hh}(\mathbf{k}_1 - \mathbf{k}_4) v_1^{\dagger} v_2^{\dagger} v_3 v_4 + V_{eh}(\mathbf{k}_1 - \mathbf{k}_4) (c_1^{\dagger} v_2^{\dagger} v_3 c_4 + v_1^{\dagger} c_2^{\dagger} c_3 v_4)], \quad (5.4)
\end{aligned}$$

where $c_{\mathbf{k}}^{\dagger}$ ($v_{\mathbf{k}}^{\dagger}$) creates an electron in the conduction (valence) band. The quantities V_{ee} , V_{hh} , V_{eh} are quantum-well interaction potentials defined in Appendix A. A Hartree-Fock decoupling of the equations of motion for $n(\mathbf{k}) = \langle c_{\mathbf{k}}^{\dagger} c_{\mathbf{k}} \rangle$ and $P(\mathbf{k}) = \langle v_{\mathbf{k}}^{\dagger} c_{\mathbf{k}} \rangle$ gives the above set of equations. This completes the proof that the real-space treatment of Stahl¹⁸ and the theories based on a k -space representation are equivalent which was already stated in Refs. 6 and 7.

Only for the Hartree term are there are differences: In our framework this term is due to a nonvanishing charge distribution along z in the quantum well (see Appendix A), whereas in Ref. 8 a probe-induced modulation in ρ space is considered.

Note that we remain in the real-time domain and do not assume stationarity. In a number of studies the following conservation law⁶ has been utilized:

$$\frac{d}{dt} \{ [1 - 2n(\mathbf{k})]^2 + 4 |P(\mathbf{k})|^2 \} = -8\Gamma |P(\mathbf{k})|^2, \quad (5.5)$$

which follows by inspection of (5.2) and (5.3). How the dephasing spoils the strict conservation was first discussed by Zimmermann.¹⁰ Noting that $n(\mathbf{k}) = 0$ and $P(\mathbf{k}) = 0$ before the arrival of a light pulse we integrate (5.5):

$$\begin{aligned}
n(\mathbf{k}, t) = & \frac{1}{2} \left[1 \pm \left(1 - 4 |P(\mathbf{k}, t')|^2 \right. \right. \\
& \left. \left. - 8\Gamma \int_{-\infty}^t dt' |P(\mathbf{k}, t')|^2 \right)^{1/2} \right]. \quad (5.6)
\end{aligned}$$

As appropriate for a pump frequency far off resonance the dephasing is often neglected when treating the pump excitation ($\Gamma_{\text{pm}}=0$). Then (5.6) is used for reducing

$$\begin{aligned}
\Delta \hbar \omega = & 2(m_0 E_{\text{pm}}^0)^2 \left(\sum_{\mathbf{k}} G(\mathbf{k}, \omega_{\text{pm}}) \phi^2(\mathbf{k}) + \sum_{\mathbf{k}\mathbf{k}'} v(\mathbf{k} - \mathbf{k}') G(\mathbf{k}, \omega_{\text{pm}}) [G(\mathbf{k}', \omega_{\text{pm}}) \phi(\mathbf{k}') + G(\mathbf{k}, \omega_{\text{pm}}) \phi(\mathbf{k})] \phi(\mathbf{k}') \right. \\
& \left. - \sum_{\mathbf{k}\mathbf{k}'} \bar{v}(\mathbf{k} - \mathbf{k}') G(\mathbf{k}, \omega_{\text{pm}}) [G(\mathbf{k}', \omega_{\text{pm}}) \phi(\mathbf{k}) + G(\mathbf{k}, \omega_{\text{pm}}) \phi(\mathbf{k}')] \phi(\mathbf{k}') \right), \quad (6.1)
\end{aligned}$$

where $v(\mathbf{k})$ and $\bar{v}(\mathbf{k})$ are Fourier transforms of $v(\rho)$ and $\bar{v}(\rho)$, $\phi(\mathbf{k})$ is the \mathbf{k} -space envelope wave function of the lowest exciton level, and $G(\mathbf{k}, \omega)$ is the \mathbf{k} -space Green's function given by

$$[\mathcal{E}_e(\mathbf{k}) + \mathcal{E}_h(\mathbf{k}) - \hbar\omega] G(\mathbf{k}, \omega) - \sum_{\mathbf{k}'} v(\mathbf{k} - \mathbf{k}') G(\mathbf{k}', \omega) = 1. \quad (6.2)$$

the temporal integration to $P(\mathbf{k}, t)$ only. In this case there remains an ambiguity with respect to the sign of the square root. It should be minus at the start time, but could switch as a function of t and \mathbf{k} whenever the radicand touches zero. This point has sometimes been overlooked⁷ and is particularly uncertain in the strictly stationary limit. A clearcut answer follows from an independent temporal integration of the equations for $n(\mathbf{k})$. Note that in the real-space representation the conservation law becomes a convolution integral from which $C(\rho)$ cannot be expressed easily in terms of $Y(\rho)$.

VI. CALCULATED RESULTS

We have calculated the optical Stark effect assuming both pump and probe pulses to be Gaussian with peak fields $E_{\text{pm}}^0, E_{\text{pr}}^0$, center frequencies $\omega_{\text{pm}}, \omega_{\text{pr}}$, and full width at half maximum (FWHM) duration for the intensity $t_{\text{pm}}, t_{\text{pr}}$, respectively. The delay of the probe pulse with respect to the pump is t_{delay} . We apply the rotating-wave approximation throughout, and the above electric field amplitudes are meant as the rotating parts only. We study the $1s$ exciton and quote absolute values related to GaAs (the bulk rydberg is equal to 4 meV, the dephasing rate near resonance $\Gamma_{\text{pr}}=1.5$ meV).

A. Perturbative treatment

For pump pulses long enough for assuming stationarity, a perturbative treatment to second order in E_{pm}^0 leads to results expressed as spectral shifts and bleaching of excitonic resonances as a function of pump field, detuning $\delta = \omega_{\text{pm}} - \omega_0$, and well width W (ω_0 is the unperturbed exciton frequency). Concentrating on the shift $\Delta \hbar \omega$ of the lowest exciton the result of such a treatment¹³ is

Assuming no pump dephasing we have calculated the shift $\Delta \hbar \omega$ for different values of the detuning δ and well width W . As $\Delta \hbar \omega$ is proportional to $(E_{\text{pm}}^0)^2$ we show in Fig. 1 the results for the dimensionless factor ϑ given by

$$\Delta \hbar \omega = \frac{2(M_0 E_{\text{pm}}^0)^2}{-\hbar \delta} \vartheta. \quad (6.3)$$

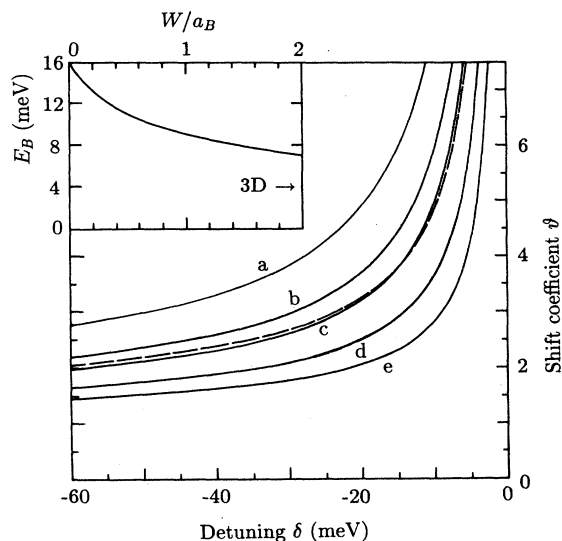


FIG. 1. Shift coefficient ϑ given in Eq. (6.3) as function of the detuning and width of an infinite barrier quantum well. The solid curves are calculated with a potential given by Eq. (3.15) with $W/a_B = 0$ (curve *a*), 0.1 (curve *b*), 0.2 (curve *c*), 0.5 (curve *d*), and 1 (curve *e*). The dashed curve refers to a homogeneous three-dimensional system, whereas curve *a* gives the corresponding two-dimensional case. The inset (upper left) shows the binding energy as a function of the relative well width W/a_B .

This implies that a two-level system has $\vartheta = 1$ (see Ref. 13). Note in Fig. 1 that the large Stark shift in a pure two-dimensional system is reduced significantly when going to a finite well width as small as $0.2a_B$ (a_B is the bulk exciton Bohr radius). The shift for W in the range $(0.2-1)a_B$ becomes even smaller than the pure three-dimensional case. This unexpected result is in clear contrast to the behavior of the binding energy (see the inset in Fig. 1) for which the interpolation between the 2D and the 3D limits is simple. Our findings indicate that the pure 2D limit is of little interest when calculating the Stark effect in real quantum-well structures. Any attempt to use the binding energy for scaling down from the 2D limit will fail.¹⁶

B. Real time numerical integration

In order to explore the optical Stark effect to higher order in E_{pm}^0 and with finite duration and dephasing time of the pump excitation, we have performed calculations based on real time integration of (3.12) and (3.13) and (4.1) and (4.2) as explained in Appendix B. We calculate two types of spectra, one based on filtering the response to a very short probe pulse with Fourier components 50 meV above and below the resonance investigated, and one based on a spectrally narrow probe pulse with no filtering after the sample.

It turns out that the two systems show very similar

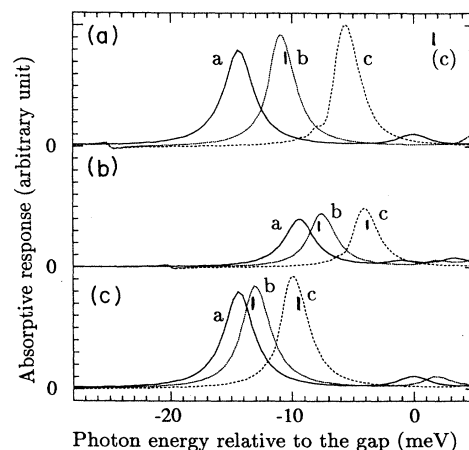


FIG. 2. Absorptive response for various values of detuning δ , peak pump fields E_{pm}^0 and width W of an infinite-barrier quantum well. The curves marked *a* are the unperturbed spectra while curves *b* and *c* have $M_0 E_{pm}^0 = 1.6$ and 3.2 meV, respectively. (a) and (c) show the spectra for the limit $W=0$ with detuning $\delta=10$ and 20 meV, respectively. In (b), $W = a_B$ and $\delta = 10$ meV. Other important parameters are $\Gamma_{pm}=0$ and $\Gamma_{pr}=1.5$ meV. The vertical bars are positioned according to shifts derived from the perturbative treatment.

behavior when the pump pulse is long (spectrally pure) enough. In this limit ($t_{pm} = 6$ ps) we find the spectra shown in Fig. 2. For Stark shifts less than 1–2 meV we find satisfactory agreement when comparing the perturbative treatment and the real-time integration in the range $0 < W < a_B$ and $-20 \text{ meV} < \delta < -10 \text{ meV}$ (see vertical bars in Fig. 2). It is seen that the perturbative

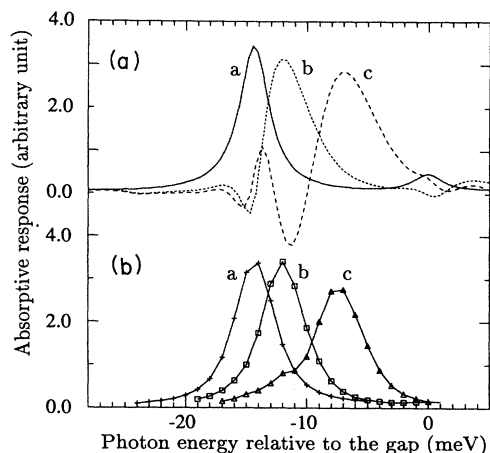


FIG. 3. Absorptive response for a finite duration ($t_{pm}=0.9$ ps) of the pump pulse. (a) shows the filtered response with a short probe pulse ($t_{pr}=20$ fs), $\delta=10$ meV, $W=0$ and pump fields given by $M_0 E_{pm}^0 = 0$ (curve *a*), 1.6 meV (curve *b*), and 3.2 meV (curve *c*). For comparison we show in (b) the corresponding unfiltered response with a spectrally narrow probe pulse ($t_{pr}=0.9$ ps) centered at the plotted frequency. The parameters for the filtered and unfiltered spectra are otherwise identical. Other important parameters are $\Gamma_{pm}=0$, $\Gamma_{pr}=1.5$ meV, and $t_{delay}=0$.

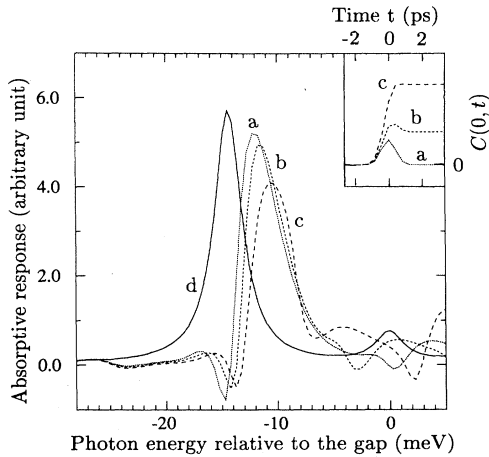


FIG. 4. Absorptive response for various values of dephasing rate Γ_{pm} of the pump excitation. The parameters are otherwise the same as for curve *b* in Fig. 3(a). The pump dephasing rate is $\Gamma_{pm}=0$ (curve *a*), 0.5 meV (curve *b*), and 1.5 meV (curve *c*). Curve *d* is the unperturbed absorption. In the upper right corner is shown the temporal behavior of the density $C(0, t)$ for the above dephasing rates.

treatment fails for the largest pump field in Fig. 2(a) because the shift in this case is comparable to the exciton rydberg. The spectra in Fig. 2 are close to the true stationary limit. A weak consequence of the finite pump pulse duration (introduced for calculational reasons) is seen as irregularities in curve *c* in Fig. 2(a). Unlike the crude two-level approximation giving strong bleaching,¹⁷ the present calculations show a slight increase of peak absorption (Fig. 2) with increasing pump field.

We then consider pump pulses with a duration of the order Γ_{pr}^{-1} (see Fig. 3). We still neglect dephasing of the pump excitation and consider zero delay. With spectral filtering after the sample the absorption peak becomes

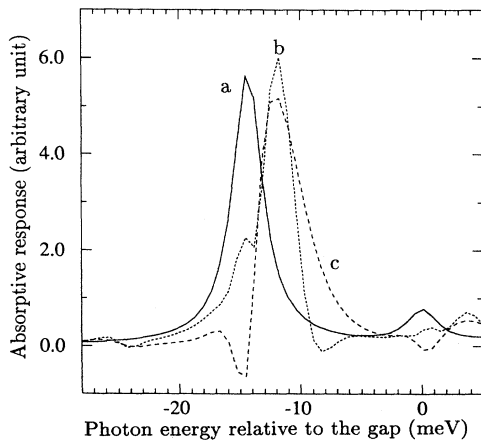


FIG. 5. Absorptive response for different values of the delay of the probe pulse. Curve *a* is valid to a good approximation for $1.5 \text{ ps} < |t_{\text{delay}}| < \infty$. The other curves have $t_{\text{delay}} = -0.65 \text{ ps}$ (curve *b*) and 0 (curve *c*). The rest of the parameters are the same as for curve *b* in Fig. 3(a).

distorted and a region with oscillatory behavior about zero absorption develops. This is the remainder of the coherent oscillations at negative delay discussed by Koch *et al.*¹¹ The effect is absent if the spectral filtering is before the sample. In any case the absorption line is less shifted and significantly broadened when compared with the steady-state result [Fig. 2(a)].

It is not meaningful in the true steady-state limit to allow a finite dephasing of the pump excitation because of the build-up of pair population. However, for finite duration of the pump pulse the influence of pump dephasing can be studied. Figure 4 shows such spectra. It is seen that noticeable changes of the Stark-shifted line set in when the total density becomes comparable to the peak density without pump dephasing, i.e. when

$$[C(0, t = 0)]_{\Gamma_{pm}=0} \approx [C(0, t = \infty)]_{\Gamma_{pm} \neq 0} \quad (6.4)$$

(the pulse is centered about $t = 0$); see the inset in Fig. 4. With the actual values of pump pulse duration, the detuning, and dephasing rate, it is seen that even in case of $\Gamma_{pm} = \Gamma_{pr}$ (which represents an unrealistically high dephasing rate of the pump), the spectra are not strongly affected by the dephasing of the pump excitation.

We finally show in Fig. 5 the influence of a nonsimultaneous arrival of the pump and probe in case of a pump pulse duration of $\approx 1 \text{ ps}$ (FWHM) and a reciprocal dephasing rate Γ_{pr}^{-1} of 0.5 ps. These results give an impression of the speed of the excitonic Stark effect in relation to potential switching applications.

It should be noted that the calculated spectral structures in Figs. 2-5 cannot be trusted at energies above about $\hbar\omega'_g - 1 \text{ meV}$ because of the cutoff in relative space at $(4-6)a_B$. On the other hand, near the lowest exciton peak the spectra are reasonably accurate. For example, the relatively coarse spatial step size of $0.2a_B$ causes an inaccuracy of $\approx 1 \text{ meV}$ in the two-dimensional limit (giving $\omega_g - \omega_0 = 15 \text{ meV}$ instead of the exact result 16 meV).

VII. DISCUSSION AND OUTLOOK

In the present work the nonlinear optical properties, particularly the optical Stark effect, have been studied using a real-space, real-time representation of a two-band density matrix theory. The real-space representation is useful for treating inhomogeneous systems such as quantum wells, while the real-time representation is unique for studying systems under influence of short external pulses (durations comparable to the typical relaxation times of the system). By separating the equations of motions for the pump and the probe excitations we allow for different dephasing rates of the two types of excitation.

Two important consequences of short pump pulses should be mentioned here. First, the detected absorption spectrum of the probe beam depends strongly on whether the spectral filtering of the probe beam is before or after the sample. The spectra with filtering after the sample suffer from a profound line distortion and from coherent oscillations on the red side of the exciton line.

Secondly, while the peak absorption of the exciton line increases with the pump field for steady state pumping, the opposite is the case for short pump pulses. Note that it is the peak absorption and the linewidth which depend on the pump pulse duration, not the integrated absorption. The calculated behavior for the short pump pulses agrees qualitatively with the experiments.^{3,4}

It should be emphasized that the input pulses used in the present study are Fourier limited. An interesting class of calculations yet to be performed concerns the influence of fluctuating phases of the incident pulses.

The quantum well specifics enter the equations only via the Coulomb potential averaged over the confinement wave functions. The simple expression (3.15) implying infinite barrier heights can be improved without much difficulty. Preliminary calculations using finite barrier heights relevant for typical $\text{Al}_x\text{Ga}_{1-x}\text{As}$ quantum wells show that the Stark shift coefficient ϑ follows the trend shown in Fig. 1. The diminished Stark shift in realistic quantum wells compared with both the pure two-dimensional and three-dimensional systems holds for finite barrier heights, too, and any linear interpolation scheme has to be abandoned. At present we have no simple physical argument for this surprising result. Note that ϑ is larger for the bulk case than realistic quantum wells. Nevertheless, for experiments on the dynamical Stark effect, the quantum wells are still superior due to their enhanced exciton oscillator strength.

A limitation of the present approach is the attachment of the interband and intraband density matrices to one sublevel only [Eqs. (3.9)–(3.11)]. This is justified as long as the excitonic correlation in the growth direction can be neglected with respect to the confinement of electron and hole within the well (the exciton binding energy small compared with the sublevel separation). For the lowest sublevel pair in $\text{Al}_x\text{Ga}_{1-x}\text{As}$, this will hold for well widths W in the range 3 nm to 25 nm which covers the major part of the quantum well structures under study.

In relation to possible applications in the field of fast optical switching, the important findings of the present work are (i) that coherent oscillations are absent if there is no filtering device after the sample, and (ii) that—as expected and confirmed in Fig. 5—the switch-off time is of the same order of magnitude as the probe dephasing time.

ACKNOWLEDGMENTS

Two of us (A.S. and R.Z.) are grateful to Odense University for hospitality during our stay. The present work has benefited from fruitful discussions with J. Hvam and from financial support from the Danish Natural Science Foundation.

APPENDIX A: QUANTUM WELL COULOMB POTENTIALS AND THE HARTREE TERM

Using units of the three-dimensional exciton, the Coulomb potential is $2/r$ and gives on integration with the

confinement wave functions

$$V_{ab}(\rho) = \int dz \int dz' \frac{2}{[\rho^2 + (z - z')^2]^{1/2}} u_a^2(z) u_b^2(z'), \quad (\text{A1})$$

the Coulomb potential matrix elements to be used for setting up the two-dimensional band-edge equations. In case of infinite confining barriers we have for sublevel index n

$$u_{e,n}(z) = u_{h,n}(z) = \left(\frac{2}{W}\right)^{1/2} \sin\left(\frac{\pi n z}{W}\right), \quad 0 < z < W. \quad (\text{A2})$$

One integration in (A1) can be carried out analytically. For equal sublevel index (relevant for allowed transitions) one obtains Eq. (3.15).

The binding potential $v(\rho)$ in (3.12) and (3.13) is equal to $V_{eh}(\rho)$ while the potential $\bar{v}(\rho)$ appearing in the exchange integral of (3.12) is given by

$$\bar{v}(\rho) = \frac{1}{2}[V_{ee}(\rho) + V_{hh}(\rho)] - h\delta(\rho). \quad (\text{A3})$$

Here the Hartree term derived from (2.17) is included as the last term in (A3). The quantity h of the Hartree term is given by

$$h = \int d^2\rho [V_{ee}(\rho) + V_{hh}(\rho) - 2V_{eh}(\rho)]. \quad (\text{A4})$$

For a strictly two-dimensional situation $h = 0$ and $v = \bar{v} = 2/\rho$. For equal sublevel indices, infinite confining barriers, and finite well width W one has $h = 0$ and the equal potentials v and \bar{v} given by (3.15).

APPENDIX B: DETAILS OF THE NUMERICAL TREATMENT OF THE BAND EDGE EQUATIONS

The calculation of the temporal development of Y , C , δY , and δC is based on a numerical integration in time of the sets of equations (3.12) and (3.13) and (4.1) and (4.2). For each time step Δt the terms contributing to the rate of change are calculated. This involves two-dimensional integrations and, in case of $\partial_t Y$ and $\partial_t(\delta Y)$ also a calculation of $\nabla^2 Y$ and $\nabla^2 \delta Y$.

In these steps a common spatial discretization with cell size $\Delta\rho$ is introduced, and the integrals and derivatives are replaced by their discretized counterpart. In the two-dimensional integrations the integration variables were transformed to be $|\rho'|$ and $|\rho - \rho'|$ before the discretization. Simpson's method was used throughout, and care was taken in treating the square-root singularities in the problem. As for the calculation of terms involving ∇^2 we use a five-point calculation giving errors higher than fourth order in $\Delta\rho$. As a pointlike function δ at the origin of relative space on the rhs of (3.12) causes divergences (related to the choice of the background dielectric

constant¹⁹) we use a ring source at $\rho = \Delta\rho$. According to the discretization, δ is replaced by a function which is zero unless the spatial counting index j ($= \rho/\Delta\rho$) is 1. The density $Y(0)$ must be calculated separately. The dominant terms in (3.12) near $\rho = 0$ are $(1/\rho)dY/d\rho$ and $v(\rho)Y$. These two terms cancel each other approximately if we put

$$Y(0) = Y(\Delta\rho)[1 + (\Delta\rho)^2 v(\Delta\rho/2)/2] \quad (\text{B1})$$

if excitonic units are used. A similar expression is used for calculating $\delta Y(0)$. The boundary condition for large r is that all densities Y , C , δY , δC vanish at a distance ρ_{\max} from the origin.

For technical reasons we transform the BEE by replacing ω'_g by $\omega'_g - \omega_{\text{pm}}$ and at the same time replace $E_{\text{pm}}, E_{\text{pr}}, Y$, and δY by the respective quantities times $\exp(i\omega_{\text{pm}}t)$. In this way the equations can be treated numerically by using time step size larger than the optical period $\approx \omega_g^{-1}$ (but much smaller than the reciprocal detuning).

The typical calculational parameters are $\Delta\rho = 0.2a_B$ (for $W = 0$) or $0.3a_B$ (for $W = a_B$), $\rho_{\max}/\Delta\rho = 20$, and $\Delta t = 1$ fs. The Fourier transformation covered the time from $3t_{\text{pr}}$ before the peak of the probe pulse to about $6\Gamma_{\text{pr}}^{-1}$ later. The typical run time for the parallel integrations of Eqs. (3.12) and (3.13) and (4.1) and (4.2) is about 1 hour on a Domain 4000 (Apollo) work station.

-
- ¹D. Fröhlich, A. Nothe, and K. Reimann, *Phys. Rev. Lett.* **55**, 1335 (1985).
²D. Fröhlich, R. Wille, W. Schlapp, and G. Weimann, *Phys. Rev. Lett.* **59**, 1748 (1987).
³A. Mysyrowicz, D. Hulin, A. Antonetti, A. Migus, W.T. Maaslink, and H. Morkoc, *Phys. Rev. Lett.* **56**, 2748 (1986).
⁴A. Von Lehmen, D.S. Chemla, J.E. Zucker, and J.P. Heritage, *Opt. Lett.* **11**, 609 (1986).
⁵S. Schmitt-Rink and D.S. Chemla, *Phys. Rev. Lett.* **57**, 2752 (1986).
⁶S. Schmitt-Rink, D.S. Chemla, and H. Haug, *Phys. Rev. B* **37**, 941 (1988).
⁷R. Zimmermann, *Phys. Status Solidi B* **146**, 545 (1988).
⁸S.W. Koch, N. Peyghambarian, and M. Lindberg, *J. Phys. C* **21**, 5229 (1988).
⁹M. Lindberg and S.W. Koch, *Phys. Status Solidi B* **150**, 365 (1988).
¹⁰R. Zimmermann and M. Hartmann, *Phys. Status Solidi B* **150**, 379 (1988).
¹¹C. Ell, J.F. Müller, K. El Sayed, L. Banyai, and H. Haug, *Phys. Status Solidi B* **150**, 393 (1988); *Phys. Rev. Lett.* **62**, 304 (1989).
¹²M. Combescot and R. Combescot, *Phys. Rev. Lett.* **61**, 117 (1988).
¹³R. Zimmermann, in *Proceedings of the 19th International Conference on the Physics of Semiconductors, Warsaw, 1988* edited by W. Zawadzki (Institute of Physics, Polish Academy of Science, Warsaw, 1989), p. 457.
¹⁴J.F. Müller, R. Mewis, and H. Haug, *Z. Phys. B* **69**, 231 (1987).
¹⁵H. Haug, J.F. Müller, and R. Mewis, *J. Luminesc.* **38**, 239 (1987).
¹⁶W. Schäfer, K.-H. Schuldt, and R. Binder, *Phys. Status Solidi B* **150**, 407 (1988).
¹⁷I. Balslev and A. Stahl, *Solid State Commun.* **67**, 85 (1988); *Phys. Status Solidi B* **150**, 412 (1989).
¹⁸A. Stahl, *Z. Phys. B* **72**, 3271 (1988).
¹⁹A. Stahl and I. Balslev, *Electrodynamics of the Semiconductor Band Edge*, Vol. 110 of *Springer Tracts in Modern Physics* (Springer-Verlag, Berlin, 1987).
²⁰Y. R. Shen, *The Principles of Nonlinear Optics* (Wiley, New York, 1984).
²¹E. Merzbacher, *Quantum Mechanics*, 2nd ed. (Wiley, New York, 1970), p. 535.
²²I. Balslev and A. Stahl, in *Optical Switching in Low-Dimensional Systems*, edited by H. Haug and L. Banyai (Plenum, London, in press).